JOURNAL OF MATERIALS SCIENCE **36** (2001) 2483–2489

A new method to evaluate material fatigue behavior

GANG QI, ENG TEIK NG
Department of Mechanical Engineering, The University of Memphis, Memphis, TN 38152-6576, USA

A new technique, the wavelet-based AE technique, was developed to investigate material fatigue behavior. In this study, an analog model was established using "clean" AE signal. The model was linearized to find the corresponding material constants. Specimens of Palacos R cement fabricated using both HM and VM methods were tested to demonstrate the proposed model. It was found that the material constants (the slopes of the test curve) were consistent regardless of the fabrication methods. However, there was a significant difference between the intercepts of the test curves when AE techniques were used, whereas the classical fracture mechanics approach failed to distinguish this difference. It was found that the slope and intercept of a test curve can be used as indicators to evaluate material fatigue behavior. In addition, the results showed that the proposed method provided a more accurate estimation of the material constant (slope) in the fatigue model.

1. Introduction

Although acoustic emission technique (AE) has been used extensively to study material fracture/fatigue behaviors and considered as a promising technique some thirty years ago, there are several factors preventing the advancement of the technique. One of the most important factors is the presence of noise in detected signals.* Under the influence of these factors, the AE technique is criticized as being unpredictable and unreliable. In this paper, the authors developed a new approach by taking the advantage of advancement in the applied mathematics. This new approach was demonstrated in the area of fracture toughness study in the author's earlier work [3–8]. The objective of the current work is to extend the previous work to the area of material fatigue behaviour study. The method used in this approach is discrete wavelet analysis.

The core of the new approach is to identify the noises and to eliminate them from the signal. There were three types of AE noises [1, 4]: environmental, internal, and special. Environmental noise is commonly known as the noise generated by external factors such as electronic instrumentation, load train, and other unidentified sources introduced from the test environment. The internal noise originates in waves other than the direct P- and S-waves, such as reflected and refracted waves. Their importance will depend, to a large extent, on the nature of the specimen investigated; the more heterogeneous the model the higher the likelihood that this kind of noise will be a problem. The last one is the special noise which are associated with particular aspects of mechanical tests and are generated by surface touching during the physical motion of the specimen. An example of this type of noise is the fretting between open surfaces associated with fatigue tests. It was claimed to be one of the most difficult noises to be eliminated/reduced [9].

Presently, the techniques to remove noise were limited to the use of threshold values for quantities such as amplitude, energy, and frequency contents. Environmental noise can be satisfactorily removed from material characterization tests. The internal noise is in the form of wave energy released during the loading process of the material. It is identified as a form of noise because it has the signal with jumbled time order due to the fact of reflected and refracted waves. It needs to be pointed out that the internal noise will usually not affect material characterization test because this type of noise is actually from the cracks/failures. The only difference between internal noise and "good" signal is that the former has a slightly mis-ordered time sequence. However, this type of noise can be a significant source of error when locating AE sources.†

The special noise, on the other hand, may or may not introduce errors in AE source location computations depending on the specific nature of each mechanical test. However, it will definitely affect the material characterization test. For example, in a mechanical fatigue test, AE signals are commonly associated with fretting noise. It is not an easy task to identify and remove this noise. In general, the crack tip region is the place where most fretting is expected. The fretting activities

* More information is provided in other publication of the author [1, 2].

† More discussions of the effects of this type of noise on an AE source location test is provided in author's other publication [1, 2].

may include the physical contact between the fatigued surfaces and acoustic signals generated by the second hand debris touching/cratching at the material surface. These activities in turn can significantly enhance the AE signal from the region of interest. It must be noted that the special noise is not in any form of stress/strain energy release during loading. Therefore, it is of no interest to include the special noise in the AE material characteristic evaluation.

In this paper, the authors developed a wavelet-based AE technique to study material fatigue behavior. The test specimens used to examine the technique were Palacos R bone cement.

2. Fatigue analog models

Fatigue behavior of material is described by the relationship between crack propagation rate and stress intensity factor. This relationship was established by the Paris Law [10] to be:

$$\frac{\mathrm{d}a}{\mathrm{d}N} = A\triangle K_{\mathrm{I}}^{\alpha} \tag{1}$$

where a is the crack length, N is the number of fatigue cycles, and A and α are material constants. $\triangle K_{\mathrm{I}}$ is the Mode I stress intensity factor range given as [11]:

$$\triangle K_{\mathrm{I}} = \frac{\triangle P}{B\sqrt{W}} f(\alpha) \tag{2}$$

where $f(\alpha)$ is called shape function and is determined by:

$$f(\alpha) = \frac{(2+\alpha)(0.886+4.64\alpha-13.32\alpha^2+14.72\alpha^3-5.6\alpha^4)}{(1-\alpha)^{3/2}} \tag{3}$$

where $\alpha = \frac{a}{W}$, W is the width of the specimen, B is the thickness of specimen, and $\triangle P = P_{\max} - P_{\min}$.

Although the parameters, A and α, in Equation 1 can be solved theoretically under extreme simplification, they are more commonly determined empirically by linearizing the equation as

$$\ln\frac{\mathrm{d}a}{\mathrm{d}N} = \alpha \ln\triangle K_{\mathrm{I}} + \ln A \tag{4}$$

where $\frac{\mathrm{d}a}{\mathrm{d}N}$ and $\triangle K_{\mathrm{I}}$ are obtained via experiments. In the linear form of Paris Law, α is the slope of the equation, whereas A is the intercept of the equation with the vertical coordinate system. In other words, the shape (or the material nature) of the relationship between the crack propagation rate and the stress intensity factor is dominated by α. The parameter A, on the other hand, controls the starting level and position of the material testing curve in this relationship. It can be seen that although both α and A are called material constants, they are not equally important. This fact becomes essential when investigating the same material fabricated under different processes. It is the interest of this paper to study the behavior of these two parameters and use them to characterize fatigue processes.

Following the same token, the relationship between AE count rate and Mode I stress intensity factor range in the conventional AE method is given by [12, 13]:

$$\frac{\mathrm{d}n}{\mathrm{d}N} = B\triangle K_{\mathrm{I}}^{\beta} \tag{5}$$

where n is the total AE counts and B and β are parameters related to material properties to be determined.

Similar effort is utilized to find the undetermined parameters B and β:

$$\ln\frac{\mathrm{d}n}{\mathrm{d}N} = \beta \ln\triangle K_{\mathrm{I}} + \ln B \tag{6}$$

$\frac{\mathrm{d}n}{\mathrm{d}N}$ in Equation 5 is the AE count rate over fatigue cyclic numbers. The count rate is measured simply by counting the number of AE signals which are above the predetermined thresholding value. The method is easy to implement. It consequently becomes the primary method being used in most AE fatigue studies. However, the frequency range of AE signal can vary from a few kHz to 2 MHz. A simple time domain threshold setting is not sufficient to eliminate various noises and disturbances in an AE test. This becomes the motive of the authors to seek a new method to compensate the disadvantages of the existing fatigue AE models.

It is not difficult to analogize that the wavelet-based AE parameter follows the same pattern defined in Equations 1 and 5 to be

$$\frac{\mathrm{d}E(t)}{\mathrm{d}N} = h\triangle K_{\mathrm{I}}^{\tau} \tag{7}$$

where $\frac{\mathrm{d}E}{\mathrm{d}N}$ is the AE energy rate. h and τ are material constants in the wavelet model. It is the main purpose of this work to determine these parameters. Linearizing the above equation, it follows:

$$\ln\frac{\mathrm{d}E}{\mathrm{d}N} = \tau \ln\triangle K_{\mathrm{I}} + \ln h \tag{8}$$

It can be seen that the main difference between Equation 5 and Equation 7 is the rate to measure the crack propagation. Instead of using a simple count rate, $\frac{\mathrm{d}n}{\mathrm{d}N}$, of AE signal, a new parameter, $\frac{\mathrm{d}E}{\mathrm{d}N}$, is proposed. This parameter inlcudes not only the information of AE signal in the time domain but the information in the frequency domain as well.[‡]

Instead of using raw AE signals, the proposed method decomposed them into a series of subsignal band. Each subsignal band has its certain frequency range. The resolution in each subsignal band varies according to the frequency value. It is one of the advantages of wavelet decomposition that the higher the frequency content is

[‡] To complete the train of thought, only a brief description is provided. More detailed treatment of the procedure is provided in other publications [4, 14, 15].

the finer the resolution in the corresponding subsignal band. This statement is expressed as [6]:

$$f(t) = f^{(0)}(t) + f^{(1)}(t) + \cdots + f^{(K)}(t) \quad (9)$$

The energy in each subsignal is measured by

$$\dot{E}^{(0)}(t) = \sum_{t=1}^{\tau} \left(f^{(0)}(\tau) \right)^2 \quad (10)$$

$$\dot{E}^{(1)}(t) = \sum_{t=1}^{\tau} \left(f^{(1)}(\tau) \right)^2 \quad (11)$$

$$\vdots$$

$$\dot{E}^{(K)}(t) = \sum_{t=1}^{\tau} \left(f^{(K)}(\tau) \right)^2 \quad (12)$$

with the total energy rate given as

$$\dot{E}^{(n)}(t) = \sum_{j} E^j \quad (13)$$

where $f^{(0)}(\tau)$, $f^{(1)}(\tau), \ldots,$ and $f^{(K)}(\tau)$ are the levels of the decomposed signal. Each component in the decomposition represents a portion of the original signal with certain frequency range in the entire time domain.

It was proved later that the slope of the test curve remain consistent regardless of the methods because it represents an intrinsic nature of the material. The intercept depends mainly on the sensitivity of the methods because it represents the difference due to the fabrication processes.

3. Experimental setup

Palacos R material was used to produce the cement block. The cement blocks were prepared via both hand and vacuum mixing methods. The cement blocks were machined to the standard compact tension specimens according to the ASTM standards E399-90 [11]. The dimension of the specimen was given in Fig. 1. A 16 mm

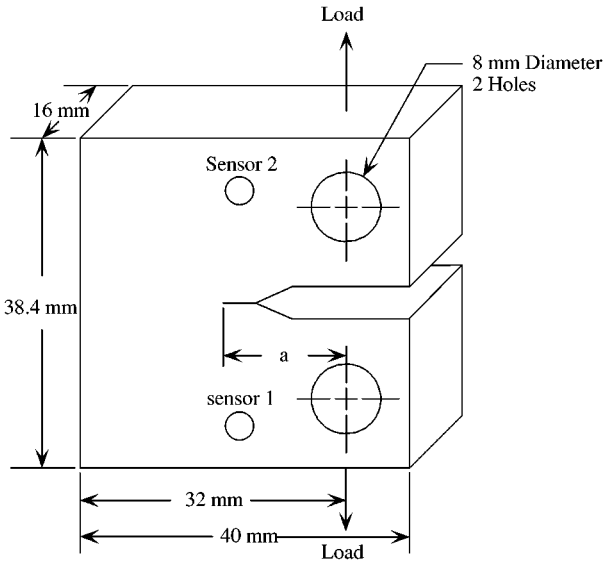

Figure 1 Compact tensile test specimen.

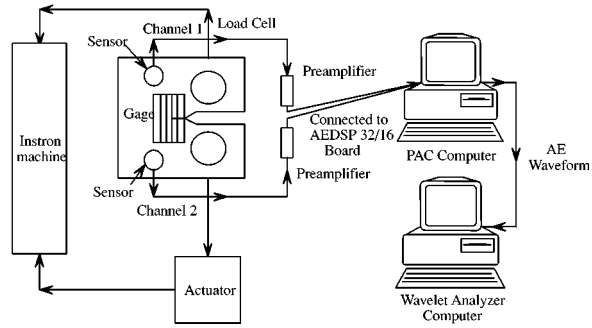

Figure 2 Experimental setup.

long thin precrack was cut using a thin blade in order to guide the crack to the instrumented area. The width ratio, a_0/W, of the crack was equal to 0.5.

All specimens were subjected to a tension-tension fatigue load using a close loop servo-hydraulic testing machine (Instron Model 8500) at room temperature. The stress ratio R was 0.1 for all tests. The loading frequency was chosen from 2 Hz to 10 Hz. The experimental setup is shown in Fig. 2.

In the tests, two wide band AE transducers were installed equidistantly on the specimen from the notch line using duct tape after cleaning the specimens with acetone. The interface between the transducers and the specimens was filled with a couplant (2211 Silicone Compound). The AE instrument used was Physical Acoustics Corporation (PAC) Mistras 2001 system. All test parameters were determined by trial and error to select the most suitable settings. These parameters were summarized in Table I. The collected AE signals were passed through a 40 dB preamplifier before entering AE instrument. The AE parameters such as counts, duration, amplitude, and energy were recorded during the tests. In addition, signal waveforms were retained for the analysis of wavelet based AE technique.

The crack length was measured separately by a regular crack propagation gage. The gage was bonded to the tip of the initial notch using M-bond AE 10 adhesive. The crack propagation signals shared the same trigger as AE equipment. In other words, both AE signals and the crack propagation data were collected

TABLE I Test parameter setup for fatigue test

	Hardware Setup Values	
Parameter Types	HM Cement	VM Cement
Thresholding Type	Float	Float
Thresholding Values	42 dB	42 dB
Peak Definition Time (PDT)	45 μs	45 μs
Hit Lock Time (HLT)	150 μs	150 μs
Hit Definition Time (HDT)	300 μs	300 μs
Sample Rate	2 MHz	2 MHz
Pre-triger	20 ms	20 ms
Hit Length	1k	1k
Cycle Counter Threshold	2.0 Volts	2.0 Volts
Filter on Board (low)	10 kHz	10 kHz
Filter on Board (high)	1.2 MHz	1.2 MHz
30 Hz Low Pass Filter	No	No
Front End Filter	No	No
Delta-T Front End Filter	Yes	Yes

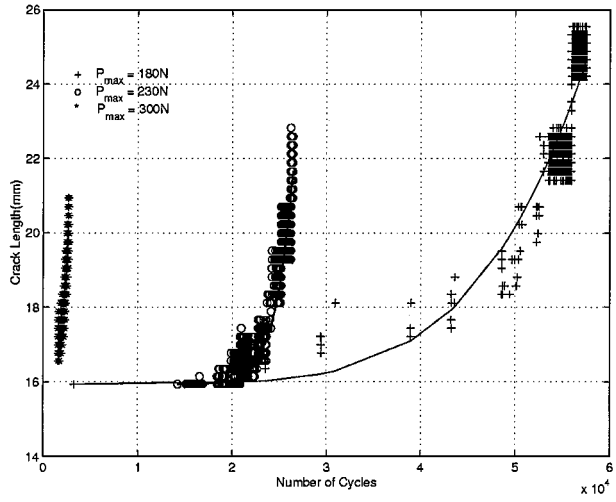

Figure 3 HM specimens crack length vs. cycle number using classical fracture mechanics approach.

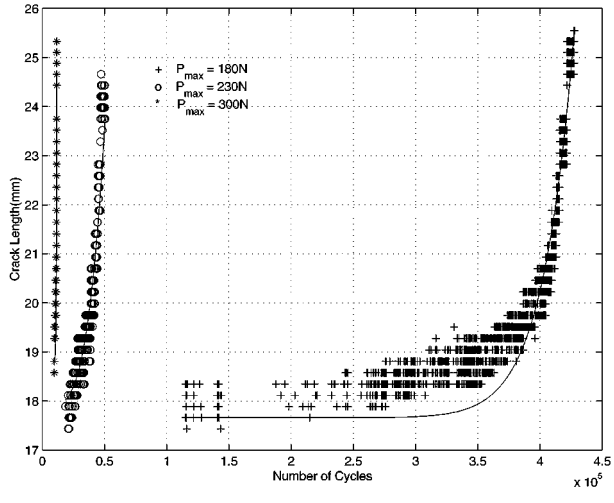

Figure 4 VM specimens crack length vs. cycle number using classical fracture mechanics approach.

simultaneously.[§] The crack propagation signal was a continuous DC output current, which is proportional to the crack length. The output was then converted to the crack length via a calibration curve provided by the manufacturer.

4. Results and discussions

The increment of the crack versus fatigue cycle numbers for HM and VM specimens are given in Figs 3 and 4, respectively. The comparison of first detectable crack, total measure crack length, and correlation coefficients are provided in Table II. The corresponding accumulative AE counts for both HM and VM specimens are given in Figs 5 and 6. The discrete wavelet analysis was applied to the AE waveforms. The wavelet-based AE results for these specimens are presented in Figs 7 and 8. Figs 9–11 show the resulting

[§]Although the crack propagation data does not require high sampling frequency because of its low resolution, 2 MHz was used to maintain the Nyquist's sampling frequency and to assure not to miss the signal from crack size as small as 10^{-3} mm.

TABLE II Comparison of crack propagation behavior for both specimens

	HM Specimen			VM Specimen		
Types	180 N	230 N	300 N	180 N	230 N	300 N
FDC (cycles)	24000	18200	1600	110000	12000	9600
TCL (mm)	25.8	23	24	24	24	23
Total Cycles (cycles)	85000	18500	2800	430000	55000	11600
Type of Curve Fitting	SOP	SOP	SOP	SOP	SOP	SOP
R^2	0.7235	0.8134	0.9013	0.9296	0.8903	0.8622

FDC: First detectable crack; TCL: total measured crack length; SOP: second order polynomial.

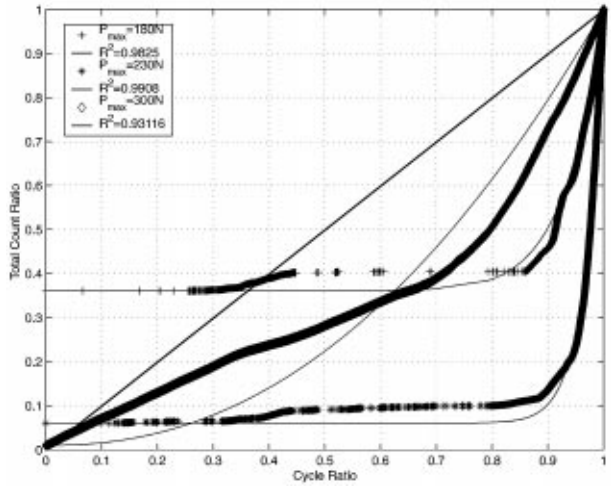

Figure 5 HM specimens AE count vs. cycle number using conventional AE approach.

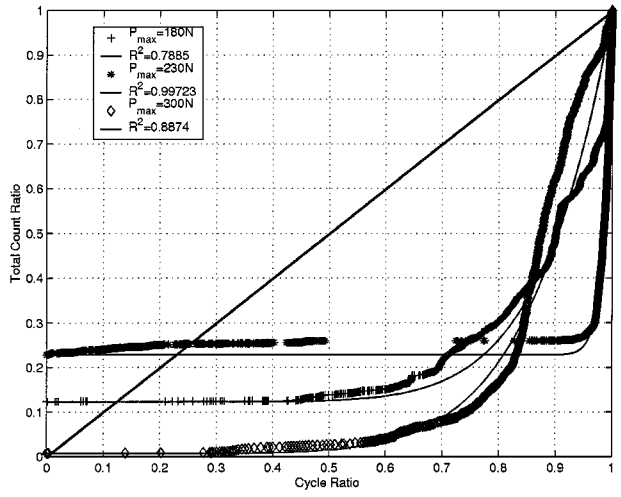

Figure 6 VM specimens AE counts vs. cycle number using conventional AE approach.

slopes and intercepts defined in Equations 4, 6, and 8, respectively. These results were normalized for comparison purposes. Table III summarizes the test results from the three different approaches.

It was found that the slopes determined by three different approaches were consistent in the following aspects. First, there was no significant difference between the values of the slopes from the test results of either specimen. This statement is obviously true because both

TABLE III Material constants determined by various methods

Method	Max Load N	HM Specimen Slope, S	HM Specimen Intercept, mm/cycle $(\text{MPa}\sqrt{\text{m}})^{-S}$	VM Specimen Slope, S	VM Specimen Intercept, mm/cycle $(\text{MPa}\sqrt{\text{m}})^{-S}$
Fracture	180	4.5668	1.0357×10^{-4}	3.9430	2.3665×10^{-4}
Mechanics	230	3.6412	3.3053×10^{-4}	4.2369	8.1020×10^{-5}
Approach	300	4.5896	8.5773×10^{-5}	3.8729	1.2789×10^{-5}
AE	180	7.0896	3.0092	5.6618	2.7097×10^{-2}
Approach	230	7.8372	3.7558	6.0219	1.8315×10^{-2}
	300	6.3079	4.9530	6.3179	2.073×10^{-2}
Wavelet-	180	5.5774	9.9576×10^{-4}	5.6562	1.6966×10^{-4}
Based AE	230	7.8362	3.4873×10^{-4}	6.0145	1.5824×10^{-5}
	300	5.2922	1.5034×10^{-3}	6.3241	1.3255×10^{-5}

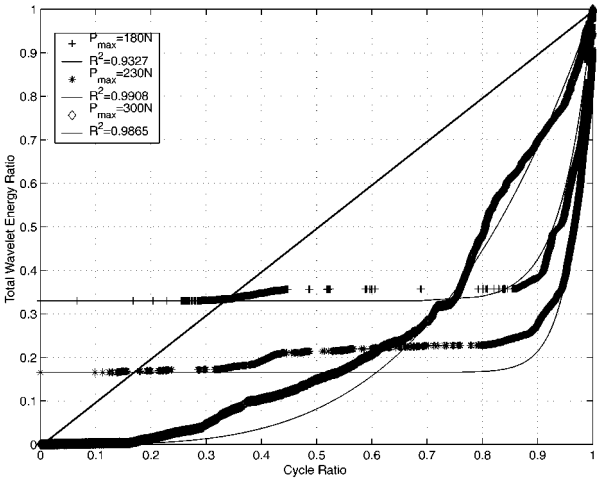

Figure 7 HM specimens AE energy vs. cycle number using wavelet-based AE approach.

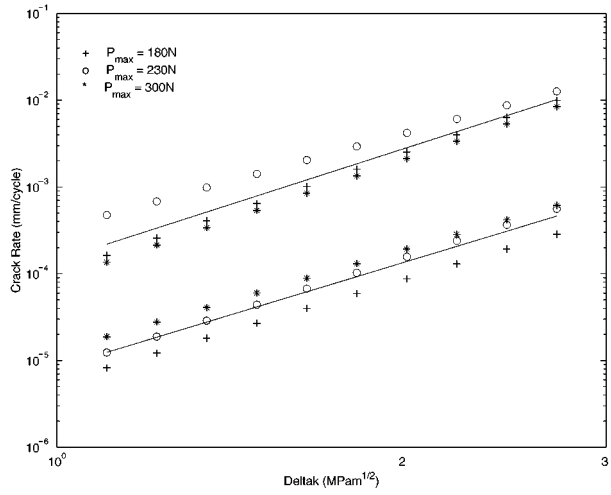

Figure 9 Linear regression between $\ln \mathrm{d}a/\mathrm{d}N$ and $\ln \triangle K$: classical fracture mechanics approach.

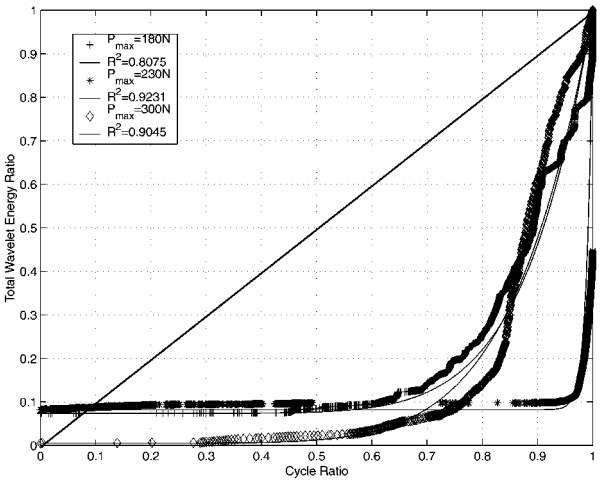

Figure 8 VM specimens AE energy vs. cycle number using wavelet-based AE approach.

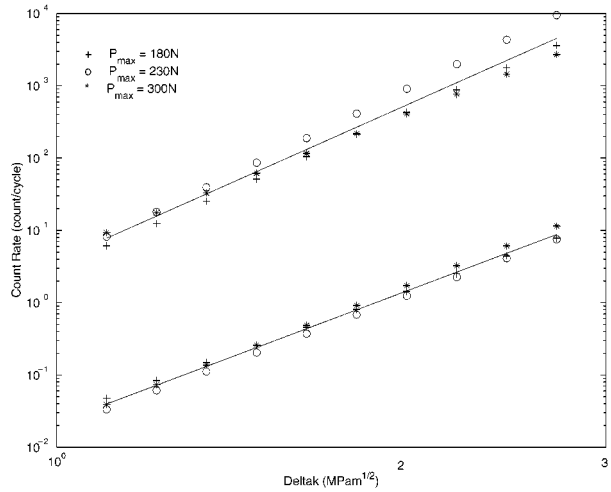

Figure 10 Linear regression between $\ln \mathrm{d}n/\mathrm{d}N$ and $\ln \triangle K$: conventional AE approach.

HM and VM specimens were made by the same material. Second, it was found $\alpha \approx \beta - 2$ for the conventional AE and $\alpha \approx \tau - 2$ for the wavelet-based AE approaches. The slopes remained consistent regardless of the methods. However, errors were existed when the results obtained from the classic fracture method was used as a base line of comparison. For instance, the slope determined by the wavelet-based AE approach had an error of only 0.49%, whereas the error was over 12% for the conventional AE. In other words, the slope determined by wavelet-based AE was closer to the ones obtained from classical fracture mechanics approach. Interestingly, the errors of conventional and wavelet-based AE approaches for VM specimens were significantly small. Although it was unclear the cause of errors, the factors such as special and internal noises in the tests of HM specimens may play some roles which

TABLE IV Comparison of the slope calculated by various methods

	Paris Model		AE Model		Wavelet Based AE Model	
Specimen	α	Er	β	$E\mathrm{r} = \frac{\beta-(\alpha+2)}{\alpha} \times 100\%$	τ	$E\mathrm{r} = \frac{\tau-(\alpha+2)}{\alpha} \times 100\%$
HM	4.2659	0	7.0782	12.9638	6.2353	0.4883
VM	4.0176	0	6.0005	0.2094	5.9983	0.3207

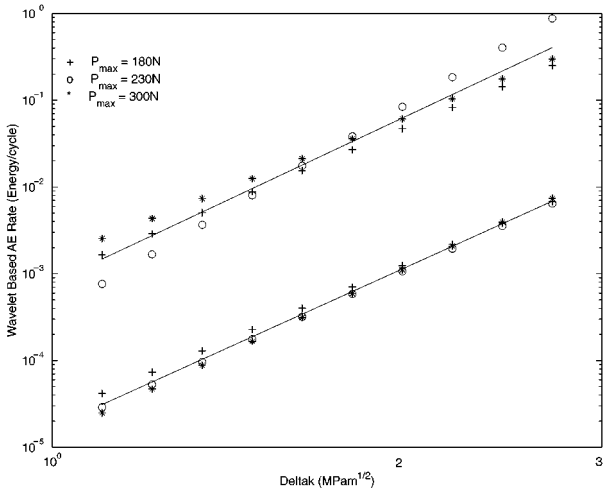

Figure 11 Linear regression between ln dE/dN and ln $\triangle K$: wavelet-based AE approach.

contributed to this error. As a result, the AE activities may be overcounted.

It was understood that the slopes should remain consistent because the specimens were made from the same material as it was proved in the tests. It was found, however, that the vertical intercepts were statistically inconsistent between the different approaches. Examining Table III, it was observed that there was no significant difference between the intercept values of HM and VM specimens obtained by the classical fracture mechanics approach. On the other hand, there was a significant difference when the AE techniques were used. Apparently, there exists an inconsistency between classical fracture mechanics and AE techniques. The authors believed that this inconsistency was due to the natural shortcoming of the classical fracture mechanics approach. It was because the classical fracture mechanics approach provided a macro-view of the material fatigue behavior in terms of the fatigue cycle numbers. The resolution of the instrument (Instron Machine for example) was considerably low. Therefore, the sensitivity to the microstructure changes was correspondingly low. In the light of this fact, the disadvantages of the classical fracture mechanics approach are: 1) insensitive to the microstructural changes in the material, and 2) unable to distinguish the difference between the fabrication processes such HM and VM methods.

However, the AE technique monitors the sonic signal from a newly created surface due to a crack. The size of the new crack may be as small as 10^{-3} mm. Consequently, AE technique overcomes the insensitivity shortcoming of the classical fracture mechanics. But, it produces a side effect at the same time that the AE technique is so sensitive such that it brings extra noises into the signal. It again answers the question that why the wavelet-based AE technique is needed. With these facts, the question of inconsistent intercepts determined by the classical fracture mechanics and AE techniques approaches can be answered in the following manner. The intercept is a material constant which does not determine the shape of the function of the material fatigue behavior. It is a constant to set the starting point and the position of the material fatigue function. In other words, it sets the material fatigue function's position in a coordinate system. In a material fatigue test, it can be an indicator to point out the differences between various fabrication processes of the material (for example, the bone cement), or some other processes which are not related to the change of material's nature. In the case of bone cement, the classical fracture mechanics method failed to realize the difference of intercepts between HM and VM specimens. This shortcoming may explain the contradictory research findings found in the literature [16–19] to some extend.

5. Summary

To summarize, this paper demonstrated a new approach in the study of material fatigue behavior. There are two main conclusions of the present study. First, the wavelet-based AE approach provides a powerful tool to eliminate the noises in AE signal. It, therefore, provides a more accurate approximation of material property, namely, the slope which is used to establish the relationship between crack propagation and stress intensity factor range. Second, AE techniques provide a way to identify the difference of various material fabrication processes. AE techniques overcome the shortcoming of the classical fracture mechanics' insensitivity to the microstructural change in the material.

Acknowledgement

This work is partially supported by the Faculty Research Grant of The University of Memphis.

References

1. G. QI and J. PUJOL and Z. F. FAN, *Journal of Biomedical Materials Research* **52**(1) (2000) 256.
2. G. QI and J. PUJOL, *Journal of Acoustic Emission* **17**(3/4) (1999) 111.
3. G. QI, in 42nd Acoustic Emission Working Group Meeting, Princeton, NJ, June 1999.
4. *Idem., NDT & E International* **33**(3) (2000) 133.
5. G. QI, A. A. BARHORST and J. HASHEMI, In VIII International Congress on Experimental Mechanics, Nashville, TN, June 1996, p. 242.
6. G. QI and A. A. BARHORST, *Engineering Fracture Mechanics* **58**(4) (1997) 363.

7. G. QI, A. A. BARHORST, J. HASHEMI and G. KAMALA, *Composites Science and Technology* **57**(4) (1997) 389.
8. G. QI and E. T. NG, in ASNT Spring Conference and 8th Annual Research Symposium, Orlando, FL, March 1999, p. 49.
9. D. FANG and A. BERKOVITS, *Journal of Acoustic Emission* **11**(2) (1993) 85.
10. P. PARIS and F. ERDOGAN, *Journal of Basic Engineering* **85** (1968) 528.
11. ASTM. ASTM E399-90. ASTM Standard, 1990.
12. M. N. BASSIM, S. ST. LAWRENCE and C. D. LIU, *Engineering Fracture Mechanics* **47**(2) (1994) 207.
13. F. HAMEL, J. P. BAILON and M. N. BASSIM, *ibid.* **14**(4) (1981) 853.
14. E. T. NG, PhD thesis, The University of Memphis, 2000.
15. E. T. NG and G. QI, *Engineering Fracture Mechancis*, In press.
16. D. HANSEN and J. S. JENSEN, *Acta Orthop Scand* **63**(1) (1992) 13.
17. S. SMEDS and D. GOERTZEN, *Clinical Orthopaedics and Related Research* (334) (1997) 326.
18. M. M. VILA, M. P. GINEBRA, F. J. GIL and J. A. PLANELL, *Journal of Biomedical Materials Research (Applied Biomaterials)* **48** (1999) 128.
19. R. L. WIXSON, E. P. LAUTENSCHLAGER and M. A. NOVAK, *Journal of Arthrop.* **2** (1987) 141.

Received 12 May
and accepted 15 November 2000